# DEVELOPING A HYBRID ACCELERATING STRUCTURE BASED ON SHORT-PULSE STRUCTURE WAKEFIELD ACCELERATION *

G. Chen†, P. Piot, J. Power,
Argonne National Laboratory, Lemont, IL, USA
C. Jing[1], Euclid Techlabs LLC, Bolingbrook, IL, USA
[1] also at Argonne National Laboratory, Lemont, IL, USA

*Abstract*

Accelerating structures powered by ultra-short RF pulses (~10 ns) at the Argonne Wakefield Accelerator (AWA) has demonstrated effective suppression of RF breakdowns and achieved gradients exceeding 400 MV/m at X-band frequencies. To fully exploit the benefits of this short RF pulse operation, an accelerating structure must simultaneously achieve two goals: high group velocity ($v_g$) to ensure rapid RF filling, and simultaneously maintain high shunt impedance ($r$) for efficient beam energy gain. Conventional accelerating structures involve inherent tradeoffs between these parameters, and limit their effectiveness in the short-pulse regime. To this end, we developed a hybrid structure composed of two co-optimized traveling wave (TW) sub-structures fed by one coupler at the middle: one backward wave (BW) filling and one forward wave (FW) filling sub-sections. This design not only preserves the short-pulse advantage, but also boosts the beam's energy gain by effectively doubling the acceleration length without requiring extended RF pulse duration. In this work, we present the RF design of the X-band (11.7 GHz) hybrid BW-FW structure in detail.

## INTRODUCTION

Short-pulse RF operation has recently gained increasing attention as a promising path toward high-gradient acceleration, with effective suppression of RF breakdown and demonstrated gradients exceeding 400 MV/m at X-band frequencies. At AWA, the short RF pulses is generated in a structure wakefield acceleration (SWFA) scheme through two-beam acceleration (TBA) technique, where a high-charge drive beam passes through a power extraction and transfer structure (PETS) to produce RF pulses with pulse lengths at the level of ~10 ns [1]. This short-pulse regime, however, introduces new challenges for the accelerating structure design. The structure must provide sufficient active acceleration length for meaningful energy gain while still being filled within the short RF duration (~ 10 ns), which requires a high group velocity ($v_g$). At the same time, a high shunt impedance ($r$) is also needed to achieve high beam energy gain for a given input power.

However, conventional metallic disk-loaded TW structures present an inherent trade-off between $r$ and $v_g$: while reducing iris size increases $r$ but weakens cell-to-cell coupling and lowers $v_g$, thus resulting in longer filling time that conflicts with the short (ns-scale) RF pulse operation. This trade-off has driven the exploration of novel structure designs that can achieve high $v_g$ while preserving high $r$. A few promising design concepts include: 1) introducing magnetic coupling slots between cells in the conventional metallic structure to increase $v_g$ [2]; 2) parallel filling structures that distribute RF power to each cell along the full accelerating structure, effectively reducing filling time while maintaining $r$ [3,4]; 3) dielectric disk-loaded structures that employ high-permittivity, RF-transparent materials to enhance both $r$ and $v_g$, though require careful tuning of the dielectric constant, since the RF properties are greatly correlated to the intrinsic material properties [5].

Beyond improving $v_g$ and $r$ within a single structure, in this work, we propose a novel architecture-level design: a hybrid TW structure composed of two halves, one backward-wave (BW) filling sub-section and one forward-wave (FW) filling sub-section, fed by a middle coupler, with each sub-section optimized for both high $r$ and $v_g$. By filling the two sub-sections simultaneously, the structure further doubles the active acceleration length and energy gain without increasing the RF pulse duration. The RF design is presented in the following section.

## STRUCTURE RF DESIGN

Figure 1 shows the design overview of the proposed hybrid BW-FW structure, including the major RF components involved in the optimization and design. The BW and FW single-cell designs are the core of the RF optimization, as they together set the overall performance of the full structure, including its operating frequency, $v_g$, $r$, and maximum achievable structure length. The BW half adopts the magnetic-coupling slot design, while the FW half adopts the parallel-filling concept to achieve high $v_g$. The remaining components such as the matching cells/slots, rectangular-to-circular waveguide adapter, and H-/E-plane power dividers, shown in insets (c)-(e) of Fig. 1 are then designed subsequently based on the optimized BW and FW geometries.

From a system-level perspective, our design prioritizes structures with high $v_g$. Since the attenuation parameter of a TW structure is given by $\alpha = \omega/(2v_gQ)$, a higher $v_g$ reduces the attenuation per unit length and enables faster RF energy propagation. This relaxes the need for complex constant-gradient geometries, in which the cell dimensions are tapered

* This work is supported by the Physical Sciences and Engineering (PSE) Early Investigator Named Award (EINA) program at Argonne National Laboratory, under contract DE-AC02-06CH11357.
† b288079@anl.gov

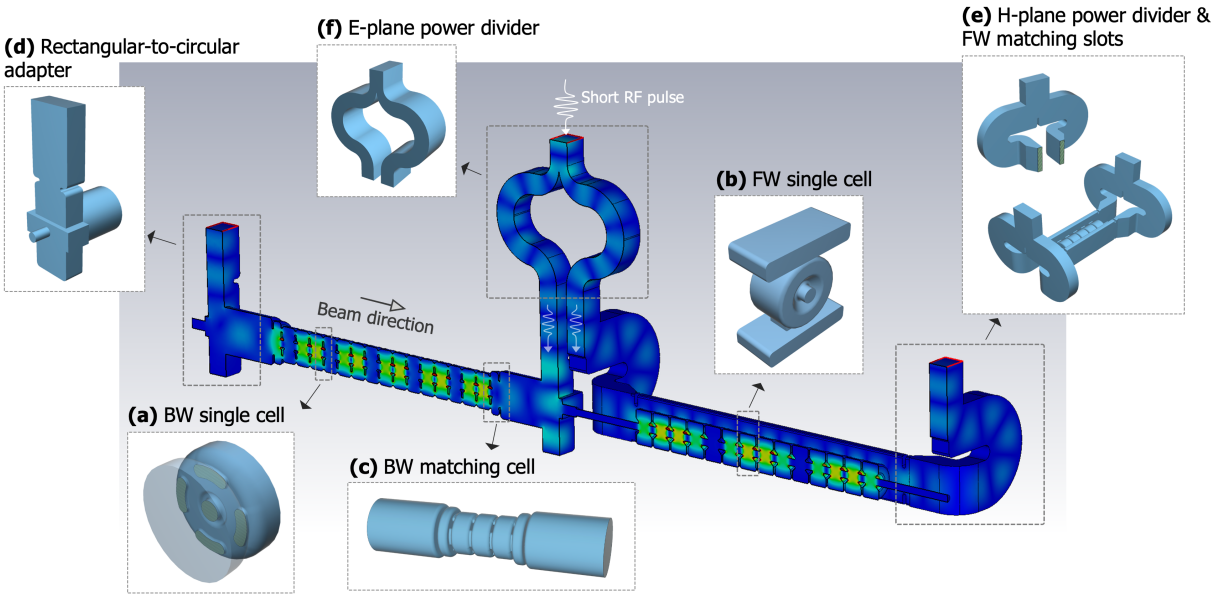


Figure 1: RF design overview of the hybrid BW-FW accelerating structure. Insets (a)-(f) show the base models of the main RF components used in the design and optimization: (a) BW single-cell, (b) FW single-cell, (c) BW matching cell, (d) WR90-to-circular waveguide adapter, (e) H-plane power divider with the matching slots, and (f) E-plane divider.

to compensate for RF power loss along the structure. For a constant impedance structure, the unloaded energy gain ($V_0$) can be expressed as,

$$V_0 = \sqrt{2rLP}\frac{1-e^{-\tau}}{\sqrt{\tau}}\,, \tag{1}$$

where $L$ is the structure length, $P$ the input RF power, and $\tau = \alpha L$ is the attenuation parameter. Under the assumptions of fixed operating frequency, comparable $Q$, and similar attenuation factor among different designs, Eq. 1 suggests the approximate scaling relation,

$$V_0 \propto \sqrt{r v_g P}. \tag{2}$$

Thus, for a given input RF power, this scaling suggests that increasing both $r$ and $v_g$ improves the achievable energy gain. Accordingly, the BW and FW single-cell optimizations focus on maximizing both quantities, as detailed in the following subsections.

### *BW Single-cell*

The BW sub-structure employs a magnetic-coupling slot design. In this work, we incorporate four magnetic-coupling slots, symmetrically arranged around the center, to mostly enhance the inner cell coupling and thus to increase $v_g$. Figure 2 illustrates the base model for the BW single-cell, showing a few key geometric parameters that will be systematically adjusted to achieve optimal performance in terms of $v_g$, $r$, and correct operating frequency ($f$).

To explore this multi-dimensional design space, we employ a Differential Evolution (DE) algorithm that iteratively converges on geometries balancing the competing performance metrics. The key geometric parameters along with their fixed values or tuning ranges are summarized in Table 1.

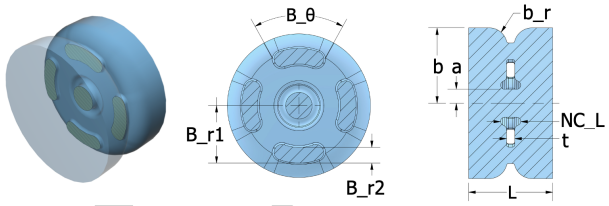


Figure 2: The single-cell base model for the BW sub-structure, showing selected parameters used for optimization.

Table 1: Selected geometric parameter settings for the BW single-cell optimization

| Parameter | Value/range | Description |
|---|---|---|
| $a$ (mm) | 1.7 | Iris radius |
| $t$ (mm) | 1 | Cell-wall thickness |
| $b$ (mm) | [8, 11] | Cell outer radius |
| $b\_r$ (mm) | [1, 3.5] | Cell outer rounding radius |
| $NC\_L$ (mm) | [2, 3] | Nose-cone length |
| $B\_\theta$ (°) | [30, 60] | Coupling-slot opening angle |
| $b\_r2$ (mm) | [0.6, 2] | Coupling-slot radial extent |

As shown in Fig. 3, three common phase-advance modes ($4\pi/5$, $3\pi/4$, and $2\pi/3$) were investigated, with the resulting Pareto fronts in the $r$-$v_g$ plane. Each scatter point corresponds to one simulated geometry, and as expected, all three modes exhibit the characteristic trade-off between $r$ and $v_g$. At a reasonably high $r$ (>125 MΩ/m) level, the $2\pi/3$ mode achieves higher $v_g$, thus demonstrating a more advantageous balance than other modes on the Pareto front. A few representative designs, including the final optimized geometry, are highlighted in Fig. 3. The red star indicates the selected optimal geometry of the $2\pi/3$ mode, which achieves a high $v_g$ together with a competitive $r$, while satis-

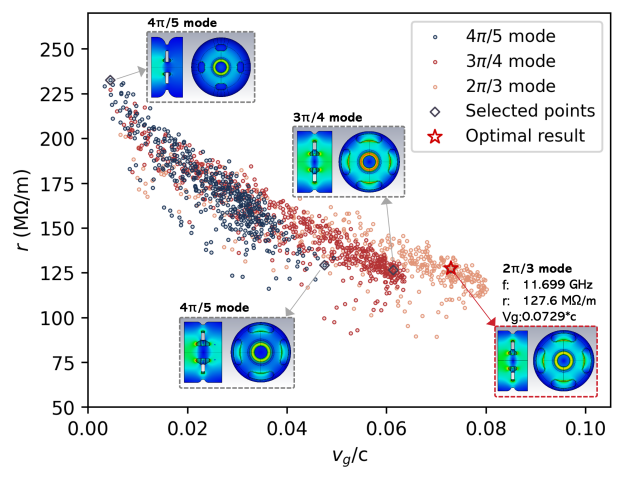


Figure 3: Pareto fronts of the BW sub-structure optimization in the $r$-$v_g$ plane for the three modes ($4\pi/5$, $3\pi/4$, and $2\pi/3$). The red star marks the selected optimal geometry; insets show representative designs with associated field distributions.

fying the frequency constraint ($r$=127.6 MΩ/m, $v_g$=0.0729c, and $f$=11.699 GHz). Given the short RF pulse duration of 6 ns (FWHM), this group velocity supports a maximum of approximately 15 fully filled cells, which determines the number of accelerating cells in the BW sub-section.

Figure 4, derived from the same optimization dataset for the $2\pi/3$-mode, provides further insight into parameter sensitivity. It reveals several clear correlations. Notably: 1) increasing the cell dome rounding ($b\_r$) generally enhances $r$ while reducing $v_g$; 2) a larger coupling slot opening angle ($B\_\theta$) tends to boost $v_g$, though with some trade-offs $r$, as also illustrated by two representative designs shown in the insets of Fig. 3. These trends offer valuable insights into the design space and highlight the critical balance between geometric modifications and performance optimization.

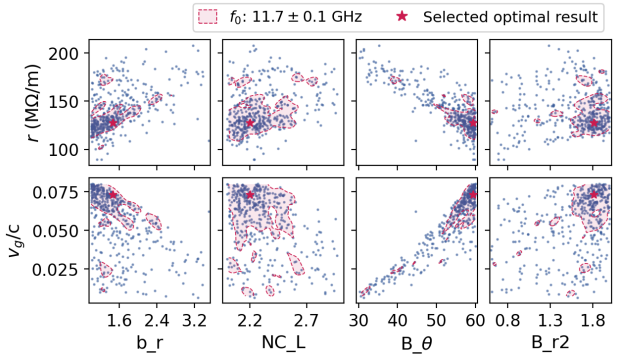


Figure 4: Parameter sensitivity analysis for the $2\pi/3$-mode BW single cell, based on the optimization data in Figure 3. Dependencies of $r$ (top) and $v_g/c$ (bottom) are shown as functions of the key geometric parameters.The shaded area indicate solution with frequencies $f \in [11.6, 11.8]$ GHz.

### *FW Single-cell*

For the FW sub-structure, we adopt the distributed parallel-filling TW design [3], in which RF power propagates along two external waveguides running parallel to the accelerating cells, above and below, and couples into each cell through dedicated holes. Figure 5 shows the base model for the FW single-cell .

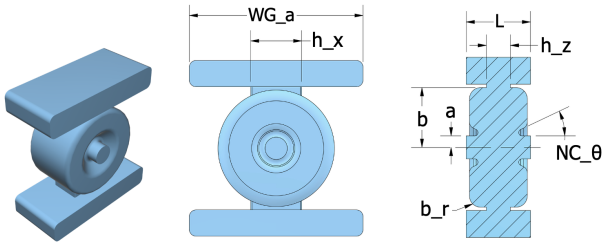


Figure 5: The single-cell base model for the FW sub-structure, showing selected parameters used for optimization.

Following the same procedure as the BW single-cell optimization, the geometric parameters listed in Table 2 were tuned within a multi-objective optimization framework, with three objectives: 1) maximizing $v_g$, 2) achieving high $r$, and 3) matching the target operating frequency of 11.7 GHz.

Table 2: Selected geometric parameter settings for the FW single-cell optimization

| Parameter | Value/range | Description |
|---|---|---|
| $a$ (mm) | 1.7 | Iris radius |
| $t$ (mm) | 1 | Cell-wall thickness |
| $WG\_a$ (mm) | 22.86 | Narrow-waveguide width |
| $b$ (mm) | [8, 11] | Cell outer radius |
| $b\_r$ (mm) | [0.5, 2.7] | Cell outer rounding radius |
| $NC\_\theta$ (°) | [45, 75] | Nose-cone angle |
| $h\_x$ (mm) | [3, 9] | Coupling-hole width |

A comprehensive exploration of the FW single-cell was also conducted on three different phase advances of $4\pi/5$, $3\pi/4$, and $2\pi/3$ to gain insight into their impact on key performance metrics. As shown in Fig. 6, across all modes, the TW parallel-filled structure demonstrates good performance overall, with the $4\pi/5$ and $3\pi/4$ modes showing slightly better performance than the $2\pi/3$ mode. Based on these results, the $4\pi/5$-mode was selected for the FW sub-strucutre. Beyond its competitive single-cell performance, operating the BW and FW halves in distinct phase-advance modes ($2\pi/3$ and $4\pi/5$, respectively) provides a natural mechanism for wakefield damping by leveraging mode interference, which may passively suppress wakefields as they propagate from one sub-structure to the other. The selected optimal $4\pi/5$-mode geometry is marked by the red star in Fig. 6, with $r$=145.6 MΩ/m, $v_g$=0.082c at the target frequency of 11.7 GHz. Given the short RF pulse duration of 6 ns (FWHM), this group velocity supports a maximum of approximately 14 fully filled cells.

Additionally, to pinpoint the key geometric drivers, Fig. 7 presents a parameter sensitivity analysis derived from the

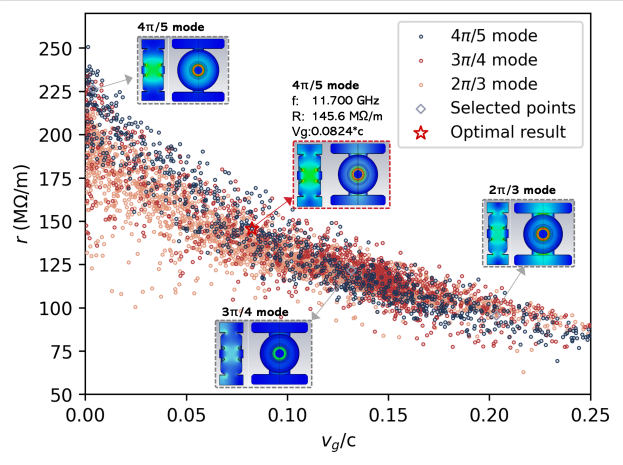


Figure 6: Pareto fronts of the FW sub-structure optimization in the $r$-$v_g$ parameter space for the three modes ($4\pi/5$, $3\pi/4$, and $2\pi/3$). The red star indicates the selected optimal geometry; insets show representative designs with associated field distributions.

optimization dataset of the $4\pi/5$ mode shown in Fig. 6. Notably, the $v_g$ exhibits a strong dependence on the coupling hole aperture ($h\_x$) along the transverse direction; with the coupling hole increases in size, $v_g$ correspondingly becomes higher, and $r$ turns lower, as also shown by selected designs in the insets of Fig. 6.

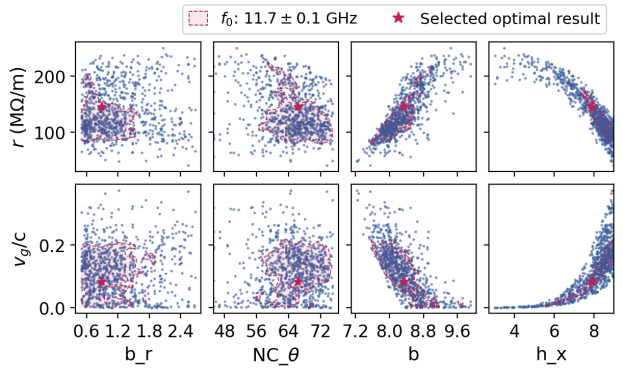


Figure 7: Parameter sensitivity analysis for the $4\pi/5$-mode FW single cell, based on the optimization data in Figure 6. The dependencies of $r$ (top) and $v_g/c$ (bottom) are shown as functions of the key geometric parameters. The shaded area indicates solution with frequencies $f \in [11.6, 11.8]$ GHz.

## *Other RF components*

With the BW and FW single-cell geometries fixed, the remaining RF components were designed accordingly.

For the BW sub-section, the matching cells shown in Fig. 1(c) adopts a conventional axi-symmetric matching cell without magnetic-coupling slots. The WR90-to-circular waveguide adapter shown in Fig. 1(d) was designed based on the idea proposed in Ref. [6]. The rectangular WR90 $TE_{10}$ mode is converted to the circular $TM_{01}$ mode via a convex transition geometry that enhances coupling to $TM_{01}$ while suppressing the lower-cutoff $TE_{11}$ mode, which would otherwise introduce undesired dipole field components.

For the FW sub-section, the H-plane power divider and matching slots shown in Fig. 1(e) were designed based on the optimized FW single-cell geometry. The slot dimensions and locations were optimized together with the H-plane power divider to achieve low reflection and a uniform field balance along the FW sub-structure.

## *Summary of the Full Structure*

Table 3 summarizes the basic RF parameters of the optimized BW and FW sub-sections. Driven by a short RF pulse of ~10 ns, the full accelerating structure is approximately 30 cm long, with both sub-sections designed to provide a balanced performance between high $v_g$, and high $r$. The normalized amplitude and phase of the on-axis electric-field profile of the full structure were simulated using CST MICROWAVESTUDIO, as shown in Fig. 8.

Table 3: Basic RF parameters of the hybrid BW-FW structure

| Parameter | BW-half | FW-half | Full structure |
|---|---|---|---|
| $f$ [GHz] | 11.7 | 11.7 | 11.7 |
| Phase advance | $2\pi/3$ | $4\pi/5$ | – |
| $v_g/c$ [%] | 7.29 | 8.24 | – |
| $r$ [MΩ/m] | 127.6 | 145.6 | – |
| $Q$ | 4243 | 5827 | – |
| Total $L$ [cm] | 12.8 \| 15-cell | 14.4 \| 14-cell | 27.2 |
| Fill time [ns] | 5.87 | 5.81 | ~5.84* |
| RF power [MW] | 300 | 300 | 600 |
| Gradient [MV/m] | 174.2 | 149.4 | ~161.8* |

*Estimated based on the two sub-sections.

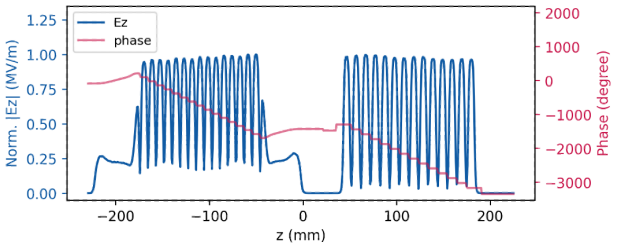


Figure 8: Normalized on-axis $E_z$ amplitude and phase as functions of longitudinal position $z$ for the X-band hybrid BW-FW structure.

This design represents an initial configuration. As indicated by the Pareto-front results in Figs 3 and 6, a wide range of different operating points exists along the $r$-$v_g$ trade-off plane for both sub-sections. Alternative designs can be selected to prioritize desired performance metrics (e.g., higher shunt impedance or faster filling) depending on the specific application.

## CONCLUSION

A novel hybrid BW-FW traveling-wave accelerating structure operating at 11.7 GHz has been proposed for short-pulse, high-gradient applications. This two-half configuration,

with RF power fed from the middle, fills both sub-sections simultaneously within the short pulse duration, effectively doubling the fillable structure length and increasing the achievable energy gain. A multi-objective Differential Evolution optimization framework was used to systematically optimize the BW and FW single-cell geometries and identify the desired operating points along the $r$-$v_g$ Pareto fronts. Based on these results, the BW $2\pi/3$-mode and FW $4\pi/5$-mode designs were selected to balance high shunt impedance and high group velocity. The full structure was then designed based on the optimized single cells, with the short ~10 ns RF pulse duration supporting a total structure length of approximately 30 cm. This design provides a promising platform for high energy-gain, short-pulse acceleration.

## FUTURE WORK

Future work will focus on refining the hybrid structure design to further increase the energy gain, and on addressing two potential challenges. The first challenge relates to wakefield studies: in the design discussed so far, the mode mismatch between the BW ($2\pi/3$) and FW ($4\pi/5$) sub-sections may suggest a way to passively damp wakefields propagating along the full structure, and dedicated simulations will quantify this effect. The second challenge concerns the transient nature of short-pulse operation where the field pattern might still be evolving while the beam undergoes acceleration (i.e., when the structure is not yet, or partially fully filled). Consequently the field profile may deviate from its steady-state profile during filling, potentially affecting beam quality [7]. Fully understanding this phenomenon and developing strategies to mitigate its impact on beam dynamics remains the focus of ongoing research.

## ACKNOWLEDGEMENTS

This work is supported by the Physical Sciences and Engineering (PSE) Early Investigator Named Award (EINA) program at Argonne National Laboratory, provided by the Director, Office of Science, U.S. Department of Energy, under contract DE-AC02-06CH11357.

## REFERENCES

[1] C. Jing, *et al.*, "Electron acceleration through two successive electron beam driven wakefield acceleration stages", *Nucl. Instrum. Methods Phys. Res. A*, vol. 898, pp. 72–76, 2018. doi:10.1016/j.nima.2018.05.007

[2] G. Chen, *et al.*, "Design and photoemission studies of a high-gradient X-band photogun operating in the short-pulse regime", *Nucl. Instrum. Methods Phys. Res. A*, vol. 1073, p. 170205, 2025. doi:10.1016/j.nima.2025.170205

[3] V. A. Dolgashev, "Traveling Wave Linear Accelerator with RF Power Flow Outside of Accelerating Cavities,"in *Proc. LINAC'16*, East Lansing, MI, USA, 2017, pp. 51–53.

[4] S. Tantawi, *et al.*, "Design and demonstration of a distributed-coupling linear accelerator structure", *Phys. Rev. Accel. Beams*, vol. 23, no. 9, p. 092001, 2020. doi:10.1103/PhysRevAccelBeams.23.092001

[5] J. Shao, *et al.*, "Study of a dielectric disk structure for short pulse two-beam acceleration", in *Proc. IPAC'18*, Vancouver, BC, Canada, May 2018. doi:10.18429/JACoW-IPAC2018-TUPML005

[6] X. Cui, *et al.*, "High-Efficiency, Broadband Converter From a Rectangular Waveguide $TE_{10}$ Mode to a Circular Waveguide $TM_{01}$ Mode for Overmoded Device Measurement", *IEEE Access*, vol. 6, pp. 14996–15003, 2018. doi:10.1109/ACCESS.2018.2815530

[7] G. Chen, P. Piot, J. Power, and C. Jing, "Short-Pulse Driven Radiofrequency X-Band Photoinjector: Electromagnetic Properties and Beam Dynamics in the Transient Regime", arXiv preprint, Mar. 2025. doi:10.48550/arXiv.2503.09575